Larger and denser: an optimal design for surface grids of EMG electrodes to identify greater and more representative samples of motor units

Arnault H. Caillet[1,2,+], Simon Avrillon[1,+], Aritra Kundu[1], Tianyi Yu[1], Andrew T.M. Phillips[2], Luca Modenese[3], Dario Farina[1]*

[1]Department of Bioengineering, Imperial College London, SW7 2AZ, UK
[2]Department of Civil and Environmental Engineering, Imperial College London, SW7 2AZ, UK
[3]Graduate School of Biomedical Engineering, University of New South Wales, Sydney, Australia

[+] These authors contributed equally to the study and share the first authorship.

* Corresponding author
Prof. Dario Farina
Sir Michael Uren Hub
Imperial College London
86 Wood Ln
London W12 0BZ
E-mail address: d.farina@imperial.ac.uk
ORCID: 0000-0002-7883-2697

Running title: HD-EMG decomposition with larger and denser grids

Abstract

The spinal motor neurons are the only neural cells whose individual activity can be non-invasively identified. This is usually done using surface grids of electromyographic (EMG) electrodes and source separation methods, i.e., surface EMG decomposition. In this study, we combined computational and experimental approaches to assess how the design parameters of grids of electrodes influence the number and characteristics of the motor units identified by EMG decomposition. We first computed the percentage of unique motor units that could be theoretically discriminated in a pool of 200 simulated motor units when recorded with grids of various sizes and interelectrode distances (IED). Increasing the density, the number of electrodes, and the size of the grids, increased the number of motor units that the EMG decomposition could theoretically discriminate, i.e., up to 83.5% of the simulated pool with a range across conditions of 30.5-83.5%. We then identified motor units from experimental EMG signals recorded in six participants with grids of various sizes (range: 2-36 cm^2) and IED (range: 4-16 mm). The configuration with the largest number of electrodes and the shortest IED maximized the number of identified motor units (56±14; range: 39-79) and the percentage of early recruited motor units (29±14%). Finally, the number of identified motor units further increased with a prototyped grid of 256 electrodes and an IED of 2 mm. These results showed that larger and denser surface grids of electrodes help to identify a more representative pool of motor units than currently reported in experimental studies.

Significance statement

Individual motor unit activities can be accurately identified by applying source separation methods to multi-channel EMG signals recorded by grids of electrodes. The design parameters of grids of EMG electrodes have never been discussed. They are usually arbitrarily fixed, often based on commercial availability. Here, we showed that using larger and denser grids of electrodes than conventionally used can drastically increase the number of identified motor units. The samples of identified motor units are moreover more balanced between early- and late- recruited motor units. Thus, these grids provide a more representative sampling of the neural activation of muscles. Gathering large datasets of motor units using large and dense grids will impact the study of motor control, neuromuscular modelling, and human-machine interfacing.

Introduction

Decoding the neural control of natural behaviors relies on the identification of the discharge activity of individual neural cells. Classically, arrays of electrodes are implanted close to the cells to record their electrical activity. The application of algorithms that separate the overlapping activity of these cells has enabled researchers to study neural processes in multiple areas of the brain (Stringer et al., 2019), such as in the motor or the sensorimotor areas (Churchland and Shenoy, 2007; Gallego et al., 2020). At the periphery of the nervous system, it is also possible to record the activity of individual motor neurons innervating muscle fibers (Heckman and Enoka, 2012; Farina et al., 2016; Enoka, 2019). The motor unit, i.e., a motor neuron and the fibers it innervates, acts as an amplifier of the neural activity, as one action potential propagating along a motor neuron's axon generates an action potential in each of the innervated muscle fibers. The activity of motor units can be identified by decomposing surface electromyographic (EMG) signals into trains of motor unit action potentials (MUAPs) using, e.g., blind-source separation algorithms (Holobar and Farina, 2014; Farina and Holobar, 2016). The multiple observations for source separation are obtained by recording EMG signals with grids of electrodes. This approach usually allows for the reliable analysis of 5 to 40 concurrently active motor units (Del Vecchio et al., 2017; Del Vecchio et al., 2020; Hug et al., 2021a).

While the design of intracortical (e.g., (Jun et al., 2017; Steinmetz et al., 2018)) and intramuscular (e.g., (Muceli et al., 2015; Muceli et al., 2022)) electrodes arrays has scaled up over the years to record larger samples of neural cells, the configuration of surface EMG grids of electrodes has not systematically evolved. Most researchers currently use grids with 64 electrodes arranged in 13 × 5 or 8 × 8 montages, the interelectrode distance (IED) between adjacent electrodes (e.g., 4 mm, 8 mm, or 10 mm) being dictated by the size of the muscle to cover. Yet, optimizing these parameters, i.e., grid size and IED, may influence the performance of EMG decomposition. Currently, there are no recommendations on optimal design parameters for grids when using surface EMG for the study of motor units.

Source separation algorithms are based on the necessary condition that identifiable motor units have unique representations across the multi-channel EMG signal (Farina et al., 2008; Holobar and Farina, 2014; Farina and Holobar, 2016). This implies that the three-dimensional waveform of a MUAP (one time dimension and two spatial dimensions) should be unique within the pool of active motor units detected by the surface grid. In practice, the identified motor units are those that innervate larger numbers of muscle fibers, as their action potentials tend to have the largest energy. Conversely, low-threshold motor units usually remain hidden since their energy is close to the baseline noise. Increasing the density of electrodes would increase the spatial sampling frequencies of the EMG signals (Farina and Holobar, 2016). This should improve the discrimination of MUAPs, allowing the identification of a larger number of motor units. Additionally, increasing the electrode density may reveal the hidden

low-threshold motor units by sampling their action potentials across a larger number of electrodes, leading to a better compensation of the additive noise in the mixture model of the EMG signal.

In this study, we combined computational and laboratory experiments to identify the optimal design criteria for grids of surface electrodes with the aim of maximizing the number of identified motor units. We first simulated a pool of 200 motor units and the associated EMG signals recorded from grids of electrodes of various sizes and densities. These simulations showed that the greater the size and the density of the grid, the higher the percentage of identifiable motor units and the relative ratio of identifiable deep units. We confirmed these theoretical results with experimental signals recorded with a grid of 256 electrodes with a 4-mm IED that was down-sampled in the space domain to obtain six grid configurations (surface range: 2-36 cm^2 and IED range: 4-16 mm). Finally, we prototyped a new grid of 256 electrodes with a 2-mm IED and demonstrated that the number of identified motor units further increased with 2-mm IED. The entire dataset (raw and processed data) and codes are available at https://figshare.com/s/f4a94d9bdff470bf10f8.

Methods

Computational study

A pool of 200 motor units was simulated to test whether increasing the density and the size of surface grids of electrodes would impact the number of identifiable motor units. The simulations were based on an anatomical model of a cylindrical muscle volume with parallel fibers (Farina et al., 2008; Konstantin et al., 2020), where subcutaneous and skin layers separate the muscle from the surface electrodes. Specifically, we set the radius of the muscle to 25.4 mm and the thicknesses of the subcutaneous and skin layers to 5 mm and 1 mm, respectively. The centers of the motor units were distributed within the cross section of the muscle using a farthest point sampling. The farthest point sampling filled the cross-section by iteratively adding centers points that were maximally distant from all the previously generated motor unit centers, resulting in a random and even distribution of the motor unit territories within the muscle. The number of fibers innervated by each motor neuron followed an exponential distribution, ranging from 15 to 1500. The fibers of the same motor unit were positioned around the center of the motor unit within a radius of 0.2 to 9.8 mm, and a density of 20 fibers/mm^2. Because motor unit territories were intermingled, the density of fibers in the muscle reached 200 fibers/mm^2. The MUAPs were detected by circular surface electrodes with a diameter of 1 mm. The simulated grids were centered over the muscle in the transverse direction, with a size ranging from 14.4 to 36 cm^2, and an IED ranging from 2 to 36 mm.

Laboratory study

<u>Participants</u>

Six healthy participants (all males; age: 26 ± 4 yr; height: 174 ± 7 cm; body weight: 66 ± 15 kg) volunteered to participate in the first experimental session of the study. They had no history of lower limb injury or pain during the months preceding the experiments. One of these individuals (age: 26 yr; height: 168 cm; bodyweight: 51 kg) participated in a second experimental session to test the prototyped grid with an IED of 2 mm. The Ethics Committee at Imperial College London reviewed and approved all procedures and protocols (no. 18IC4685). All participants provided their written informed consent before the beginning of the experiment.

<u>Experimental tasks</u>

The two experimental sessions consisted of a series of isometric ankle dorsiflexions performed at 30% and 50% of the maximal voluntary torque (MVC) during which we recorded high density electromyographical (HD-EMG) signals over the Tibialis Anterior muscle (TA). The participants sat on a massage table with the hips flexed at 30°, 0° being the hip neutral position, and their knees fully extended. We fixed the foot of the dominant leg (right in all participants) onto the pedal of a commercial

112 dynamometer (OT Bioelettronica, Turin, Italy) positioned at 30° in the plantarflexion direction, 0° being
113 the foot perpendicular to the shank. The thigh was fixed to the massage table with an inextensible 3-cm-
114 wide Velcro strap. The foot was fixed to the pedal with inextensible straps positioned around the
115 proximal phalanx, metatarsal and cuneiform. Force signals were recorded with a load cell (CCT
116 Transducer s.a.s, Turin, Italy) connected in-series to the pedal using the same acquisition system as for
117 the HD-EMG recordings (EMG-Quattrocento; OT Bioelettronica). The dynamometer was positioned
118 accordingly to the participant's lower limb length and secured to the massage table to avoid any motion
119 during the contractions.

120 All experiments began with a warm-up, consisting of brief and sustained ankle dorsiflexion performed
121 at 50% to 80% of the subjective MVC. During the warm-up, all participants learnt to produce isometric
122 ankle dorsiflexion without co-contracting the other muscles crossing the hip and knee joints. At the same
123 time, we iteratively adjusted the tightening and the position of the straps to maximize the comfort of the
124 participant. Then, each participant performed two 3-to-5 s MVC with 120 s of rest in between. The peak
125 force value was calculated using a 250-ms moving average window, and then used to set the target level
126 during the submaximal contractions. After 120 s of rest, each participant performed two trapezoidal
127 contractions at 30% and 50% MVC with 120 s of rest in between, consisting of linear ramps up and
128 down performed at 5%/s and a plateau maintained for 20 s and 15 s at 30% and 50% MVC, respectively.
129 The order of the contractions was randomized. One participant (S2) did not perform the contractions at
130 50% MVC.

131

132 <u>High-density electromyography</u>

133 In the first experimental session, four adhesive grids of 64 electrodes (13 x 5 with a missing electrode
134 in a corner; gold coated; 1 mm diameter; 4 mm IED; OT Bioelettronica) were placed over the belly of
135 the TA. The grids were carefully positioned side-to-side with a 4-mm-distance between the electrodes
136 at the edges of adjacent grids (Figure 1A). The 256 electrodes were centered to the muscle belly and
137 laid within the muscle perimeter identified through palpation. The skin was shaved, abrased and cleansed
138 with 70% ethyl alcohol. Electrode-to-skin contact was maintained with a bi-adhesive perforated foam
139 layer filled with conductive paste. The grids were wrapped with tape and elastic bands to secure the
140 contact with the skin. The four 64-pre-amplifiers were connected in-series with stackable cables to a wet
141 reference band placed above the medial malleolus of the same leg. HD-EMG signals were recorded in
142 monopolar derivation with a sampling frequency of 2,048 Hz, amplified (x150), band-pass filtered (10–
143 500 Hz), and digitized using a 400 channels acquisition system with a 16-bit resolution (EMG-
144 Quattrocento; OT Bioelettronica).

145 In the second experimental session, one ultra-dense prototyped grid of 256 electrodes (Figure 1H; 26 x
146 10 with a missing electrode in each corner; gold coated; 1 mm diameter; 9 cm^2 area; 2-mm IED; custom-

147 manufactured for this study by OT Bioelettronica) was placed over the belly of the TA and the HD-
148 EMG signals were recorded using the same procedure as previously described.

149

150 Grid configurations

151 During the first experimental session, we recorded the myoelectric activity of the TA with a total of 256
152 electrodes covering 36 cm^2 of the muscle surface (10 cm x 3.6 cm, 4-mm IED, Figure 1A). To investigate
153 the effect of the electrode density, we down-sampled the 256-electrode grid by successively discarding
154 rows and columns of electrodes and artificially generating three new grids covering the same area with
155 IEDs of 8 mm, 12 mm, and 16 mm, involving 256, 64, 35, and 20 electrodes, respectively (Figure 1B-
156 D). It is noteworthy that the 8-mm and 16-mm grids covered a surface of 32 cm^2 because they included
157 an odd number of rows and columns. To investigate the effect of the size of the grid, we discarded the
158 peripherical electrodes to generate grids of 63, 34 and 19 electrodes with a 4-mm IED, covering 7.7, 3.8
159 and 2 cm^2 of the muscle (Figure 1E-G). Note that we chose these grid sizes to match the number of
160 electrodes used in the density analysis, thus comparing grids with similar number of electrodes, but
161 different densities and sizes (in Figure 1, B versus E, and C versus F).

162 During the second experimental session, we recorded the myoelectric activity of the TA with an ultra-
163 dense grid of 256 electrodes covering 9 cm^2 of the muscle (5 cm x 1.8 cm, 2-mm IED, Figure 1H). Using
164 the same procedure as above, we generated two artificial grids of 64 and 32 electrodes with an IED of 4
165 mm and 8 mm, respectively.

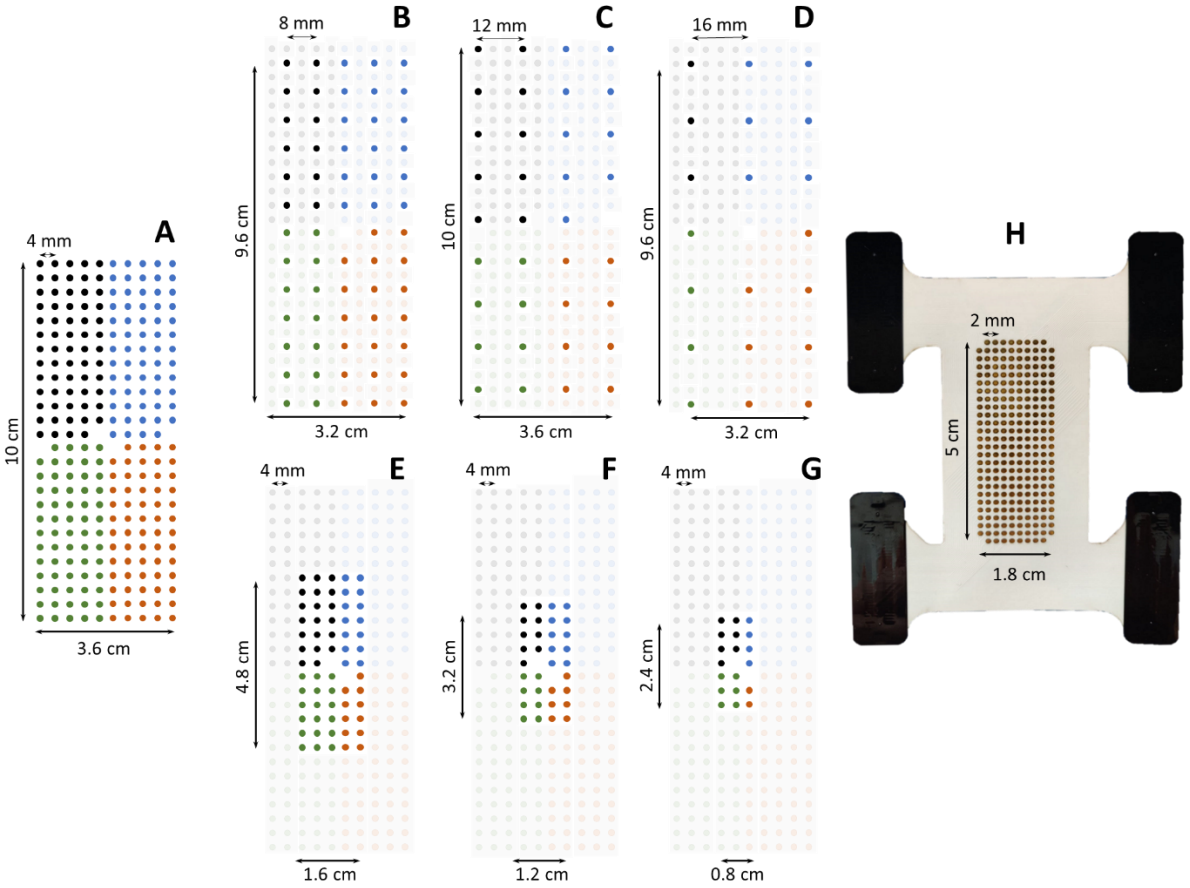

Figure 1: The eight grid configurations considered in this study. From the first grid of 256 electrodes (A, grid size: 36 cm^2, IED: 4 mm), six shallower and smaller grids (B-G) were artificially obtained by discarding the relevant electrodes. (B,C,D) Density analysis: 8, 12, and 16mm IED. (E,F,G) Size analysis: 7.7, 3.6, and 2 cm^2 surface area. (H) The ultra-dense prototyped grid of 256 electrodes (grid size: 9 cm^2, IED: 2 mm).

<u>HD-EMG decomposition</u>

We decomposed the signals recorded in all the conditions using the same algorithm, parameters, and procedure. First, the monopolar EMG signals were band-pass filtered between 20-500 Hz with a second-order Butterworth filter. After visual inspection, channels with low signal-to-noise ratio or artifacts were discarded. The HD-EMG signals were then decomposed into individual motor unit spike trains using convolutive blind-source separation, as previously described (Negro et al., 2016). In short, the EMG signals were first extended by adding delayed versions of each channel. We kept the same extension factor for all the conditions to reach 1000 extended channels, as previously suggested (Negro et al., 2016). The extended signals were spatially whitened to make them uncorrelated and of equal power. Thereafter, a fixed-point algorithm was applied to identify the sources embedded in the EMG signals, i.e., the series of delta functions centered at the motor unit discharge times. These sources are sparse, with most samples being 0 (i.e., absence of discharge) and a small number of samples being 1 (i.e.,

discharge times). In this algorithm, the contrast function g(x) = log(cosh(x)) was iteratively applied to the EMG signals to estimate and maximize the level of sparsity of the estimated sources, and the convergence was reached once the level of sparsity did not substantially vary (i.e., with a tolerance fixed at 10^{-4}) when compared to the previous iteration (Negro et al., 2016). At this stage, the estimated source contained high peaks (i.e., the delta functions from the identified motor unit) and lower values due to the activities of other motor units and noise. High peaks were separated from lower values using peak detection and K-mean classification with two classes. The peaks from the class with the highest centroid were considered as the spikes of the identified motor unit. A second algorithm refined the estimation of the discharge times by iteratively recalculating the motor unit filter and repeating the steps with peak detection and K-mean classification until the coefficient of variation of the inter-spike intervals was minimized. This decomposition procedure has been previously validated using experimental and simulated signals (Negro et al., 2016). After the automatic identification of the motor units, duplicates were removed. For this purpose, the spike trains identified from pairs of motor units were first aligned using a cross-correlation function to account for a potential delay due to the propagation time of action potentials along the fibers. Then, two discharge times were considered as common when they occurred within a time interval of 0.5 ms, and two or more motor units were considered as duplicates when they had at least 30% of their identified discharge times in common. The motor unit with the lowest coefficient of variation of the inter-spike intervals was retained for the analyses. At the end of these automatic steps, all the motor unit spike trains were visually checked, and manual edition was performed to correct the false identification of artifacts or the missed spikes (Del Vecchio et al., 2020). The update of the motor unit filters with the corrected discharge times always improved the distance between the spikes and the noise. Note that this manual step is highly reliable across operators, as previously demonstrated by Hug et al. (2021b). Only the motor units which exhibited a pulse-to-noise ratio (PNR) > 28 dB were retained for further analysis.

We further tested whether decomposing subsets of electrodes within a highly populated grid of 256 electrodes increased the number of identified motor units. Indeed, the lower ratio of large motor units sampled by each independent subset of 64 electrodes could allow the algorithm to converge to smaller motor units that contribute to the signal. For a similar number of iterations, it is likely that these motor units would have otherwise contributed to the noise component of the mixture model of the EMG signal (Farina and Holobar, 2016). Thus, we decomposed the grids of 256 electrodes (4-mm and 2-mm IED, Figure 1A, H) as four separated grids of 64 electrodes before removing the motor units duplicated between grids.

Analysis

Computational study

We first estimated the theoretical percentage of identifiable motor units for each of the simulated conditions. To do so, the simulated MUAPs detected over the entire set of electrodes were compared with each other. The comparisons were done pairwise by first aligning the MUAPs in time using the cross-correlation function, and then computing the normalized mean square difference between the aligned action potentials. Pairs of action potentials with a mean square difference below 5% were considered not discriminable. The 5% criterion was based on the variability of motor unit action potential shapes observed experimentally for individual motor units (Farina et al., 2008). After computing all pair-wise comparisons, we then computed the proportion of action potentials that could be discriminated from all others, i.e., the proportion of unique action potentials. This metrics is independent from the algorithm used for decomposition and establishes an upper bound in the number of motor units that can be identified by any decomposition algorithm. For each unique action potential, we also computed the distance between the center of the territory of the corresponding muscle fibers and the skin surface.

Laboratory study – number of identified motor units

We reported the absolute number of motor units (PNR > 28 dB) identified with all the experimental grid configurations. For each participant, the number of identified motor units was then normalized to the maximal number of motor units found across all conditions, yielding normalized numbers of identified motor units $\overline{N}$ then expressed in percentage. For each condition, we calculated the mean and standard deviation of the $\overline{N}$ values across participants. To investigate the effects of density and size of the grid, we fitted logarithmic trendlines to the relationships between the averaged $\overline{N}$ values and IED or grid size. We also fitted a logarithmic trendline to the average $\overline{N}$ values and their corresponding number of electrodes, in which case the conditions involving the same number of electrodes, but different grid size and density, were given a weight of 0.5 in the minimization function. We reported the r^2 and p-value for each regression trendline. To maintain consistency with the computational study on the investigation of the maximum number of identifiable motor units depending on grid design, the trendlines were fitted on the results obtained when the complete grids of 256 electrodes were decomposed as independent subsets of 64 electrodes, which systematically returned the highest number of identified motor units. The trendlines fitted on the results obtained when all available signals were simultaneously decomposed are reported in Extended Material A.

Laboratory study – characteristics of identified motor units

To investigate the effects of electrode density and grid size on the characteristics of the motor unit identified, we used a typical frequency distribution of the motor unit force recruitment thresholds in the human TA (Caillet et al., 2022a), where $F^{th}(j)$ is the force recruitment threshold of the jth motor unit in the normalized motor unit pool ranked in ascending order of Fth.

$$F^{th}(j) = 0.50 \cdot \left(58.12 \cdot j + 120^{j^{1.83}}\right), j \in [0; 1]$$

Based on their measured force recruitment threshold, the identified motor units were classified with this relationship to the first ('early recruitment') or second ('late recruitment') half of the active pool, consistent with the Henneman's size principle (Henneman and Mendell, 1981; Caillet et al., 2022b). For each condition, we reported the percentage of motor units with an early recruitment. We did not report this metric when five or fewer motor units were identified in one condition for three or more participants.

Laboratory study – correlation between observations

We assessed how the density of electrodes impacted the information redundancy in the EMG signals recorded by adjacent electrodes. To this end, MUAP shapes were identified over the 256 electrodes with the spike-triggered averaging technique. To do so, the discharge times were used as a trigger to segment and average the HD-EMG signals over a window of 50 ms. For each motor unit, we identified the electrode with the highest MUAP peak-to-peak amplitude and calculated the average correlation coefficient ρ with the MUAPs recorded by the four adjacent electrodes using an IED of 4 mm, 8 mm, 12 mm, and 16 mm. We also repeated this correlation analysis for the ultra-dense grid of 256 electrodes using an IED of 2 mm, 4 mm, and 8 mm.

Results

All the datasets (raw and processed data) and codes used to process the data are available at https://figshare.com/s/f4a94d9bdff470bf10f8.

Computational study

We simulated the discharge activity of 200 motor units recorded by 84 configurations of grids of electrodes (Figure 2; surface range: 14.4 to 36 cm^2, IED range: 2 to 36 mm). The number of identifiable motor units increased with the surface size of the grid, from 46.7 ± 7.7% of the motor units identifiable with a grid of 14.4 cm^2 to 77.8 ± 5.5% of the motor units identifiable with a grid of 36 cm^2. The number of identifiable motor units also increased with shorter interelectrode distances. For example, with a grid of 36 cm^2, the number of identifiable motor units increased from 63.5% to 83.5% of the motor units with an IED of 36 and 2 mm, respectively (Figure 2B). Increasing the surface size and the density of the grid of electrodes revealed deeper motor units. The averaged distance of identifiable motor units from the skin increased with the surface size of the grid (Figure 2C; 14.3 ± 0.1 mm vs. 16.5 ± 0.2 mm with grids of 14.4 and 36 mm^2, respectively), but not with the IED of the grids (Figure 2D; 15.6 ± 1.1 mm vs. 15.5 ± 0.9 mm with an IED of 36 and 2 mm, respectively).

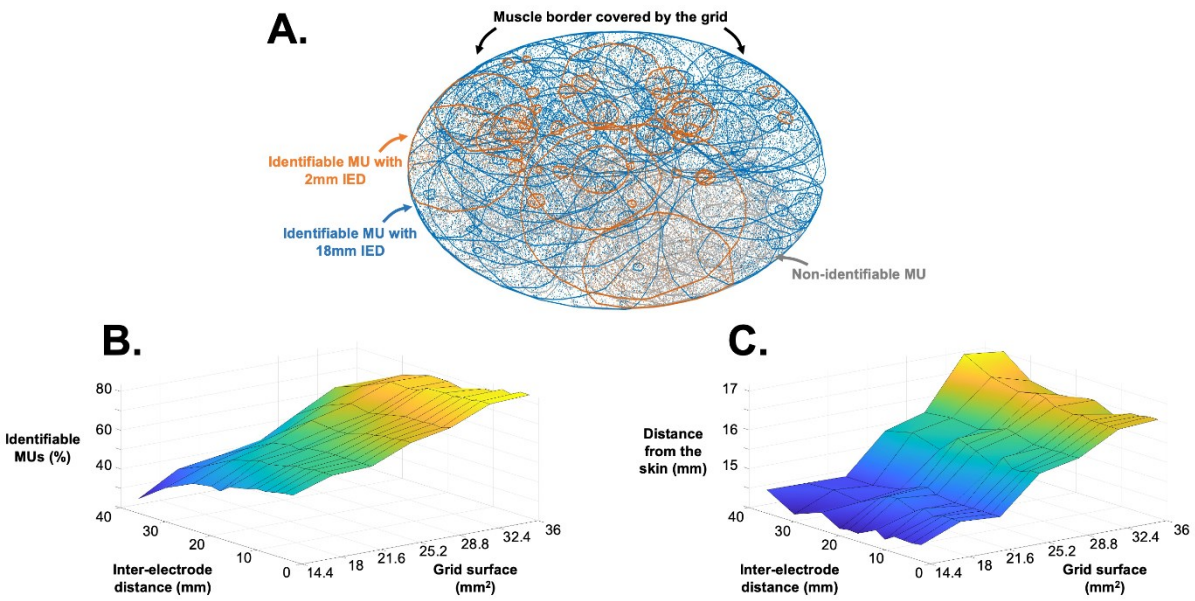

Figure 2: Results from the 200 simulated motor units with 84 configurations of grids of electrodes. (A) Each solid line represents a motor unit territory, the scatters being the muscle fibers. Blues lines are the identifiable motor units with a grid of 21.6 cm^2 and an interelectrode distance (IED) of 18 mm, while the orange lines are the motor units revealed with a grid of 21.6 cm^2 and an IED of 2mm. Grey lines represent the non-identifiable motor units. The percentage of identifiable motor units (B) and their distance from the skin (C) are reported for the 84 configurations.

Laboratory study - grids of 256 electrodes with an IED of 4-mm

Number of identified motor units

The motor unit spike trains identified across all conditions, intensities, and participants were visually checked and carefully edited when a missing spike or an identified artifact were observed. The highest number of identified motor units was systematically reached with the separate decomposition of the four grids of 64 electrodes with an IED of 4 mm, resulting in 56 ± 14 motor units (PNR = 34.2 ± 1.1) and 45 ± 10 motor units (PNR = 34.0 ± 0.9) for 30% and 50% MVC, respectively (Figure 3). At least 82% of the motor units identified in one condition were also identified in the conditions involving a higher number of electrodes. Similarly, 91% to 100% of the motor units identified in one condition were also identified with the 256-electrode configuration (4-mm IED, 36-cm^2 size, Figure 1A) when the four grids were decomposed separately.

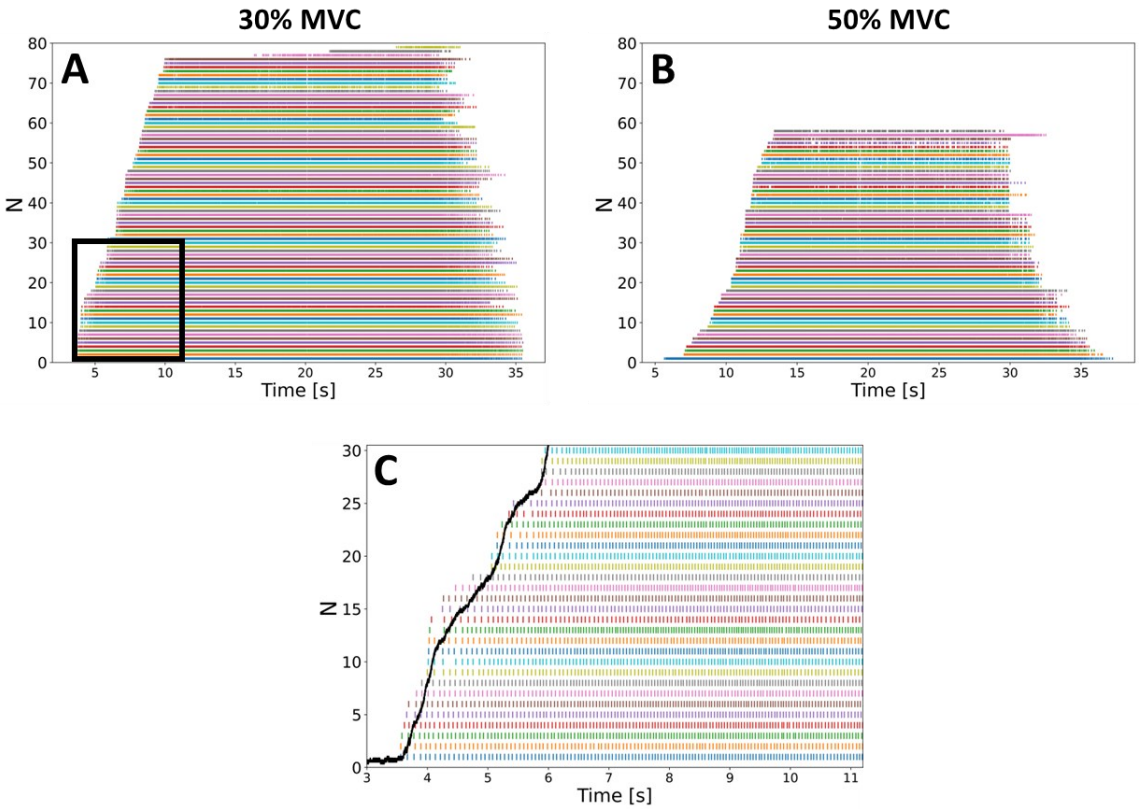

Figure 3: Maximum number of motor unit spike trains identified in one participant (S1) at 30% (A) and 50% MVC (B), with 79 and 58 motor units, respectively. They were identified with a separate decomposition of the four grids of 64 electrodes (4 mm IED). (C) The discharge times of the 30 first recruited motor units during the ascending ramp of force (black curve) at 30% MVC (black box in A).

When considering the effect of electrode density (grid size fixed at 32-36 cm^2, Figure 1A-D), we found the lowest number *N* of motor units with the 16-mm IED, identifying 3 ± 1 motor units and 2 ± 1 motor units at 30% and 50% MVC, respectively (Figure 4A, C). Additional motor units were then gradually

identified with greater electrode densities. The highest number of motor units was observed with the highest density (4-mm IED), respectively identifying 56 ± 14 or 43 ± 11 motor units and 45 ± 10 or 25 ± 6 motor units at 30% and 50% MVC, and this with the 4×64 or 256-electrode decomposition procedure (Figure 4A, C). Finally, we found a decreasing logarithmic relationship between the average normalized number $\overline{N}$ of motor units for each participant and the IED, with $r^2 = 1.0$ ($p = 2.5 \cdot 10^{-5}$) and $r^2 = 0.99$ ($p = 0.001$) at 30% and 50% MVC, respectively (Figure 4B, D).

When considering the effect of the size of the grid (IED fixed at 4 mm, Figure 1A, E-G), we found the lowest number N of motor units with a grid of 2 cm^2, identifying 4 ± 2 motor units and 4 ± 2 motor units at 30% and 50% MVC, respectively (Figure 5A, C). Additional motor units were then gradually identified with larger grid sizes. The highest number of motor units was observed with a grid of 36 cm^2, respectively identifying 56 ± 14 or 43 ± 11 motor units and 45 ± 10 or 25 ± 6 motor units at 30% and 50% MVC, depending on the decomposition procedure (Figure 5A, C). We also found an increasing logarithmic relationship between the average normalized number $\overline{N}$ of motor units for each participant and the size of the grid, with $r^2 = 0.99$ ($p = 3.0 \cdot 10^{-4}$) and $r^2 = 0.98$ ($p = 0.001$) at 30% and 50% MVC, respectively (Figure 5B, D). It is noteworthy that, in both density and size cases, the parameters of the fits were very similar for 30% and 50% MVC.

As both the density and the size of the grids determine the number of electrodes, we finally fitted the relationship between the normalized number of motor units $\overline{N}$ and the number of electrodes. As observed previously, more motor units were identified with a larger number of electrodes, following a logarithmic tendency with $r^2 = 0.98$ ($p = 0.018$) and $r^2 = 0.95$ ($p = 0.016$) at 30% and 50% MVC, respectively (Figure 6). A plateau should theoretically be reached with highly populated grids of 1024 and 4096 electrodes (36-cm^2 grids with 2-mm and 1-mm IED, respectively), with a prediction of 50% and 90% of additional motor units identified.

For a fixed number of electrodes, it is noteworthy that grid size and density, although linked, may have different impact on the number of identified motor units (black crosses in Figure 6). For example, 1.25 times more motor units were obtained with the 64-electrode condition (32 cm^2, 8-mm IED, Figure 1B) than with the 63-electrode condition (7.7 cm^2, 4-mm IED, Figure 1E) for the group of participants at 30% MVC.

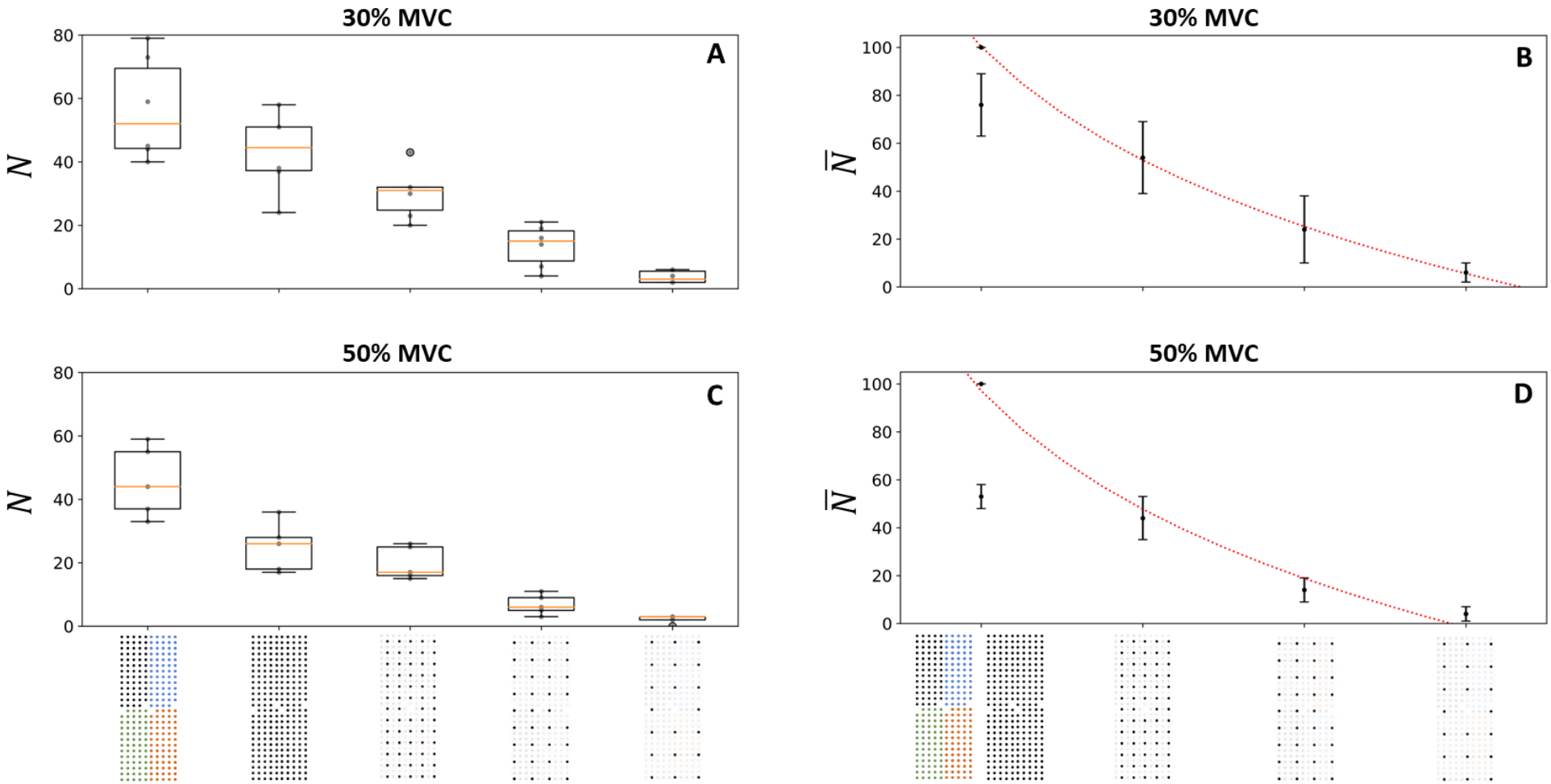

Figure 4: Effect of the electrode density on the number of identified motor units N at 30% (A, B) and 50% MVC (C, D). The boxplots in the left column report the absolute number N of identified motor units per participant (grey dots) and the median (orange line), quartiles, and 95%-range across participants. In the right column, the normalized number of motor units $\overline{N}$ logarithmically decreases with interelectrode distance d (4, 8, 12, and 16mm in abscissa) as $\overline{N} = 195 - 68\,log(d)$ $(r^2 = 1.0, p = 2.5 \cdot 10^{-5})$ at 30% MVC (B) and $\overline{N} = 196 - 71\,log(d)$ $(r^2 = 0.99, p = 0.001)$ at 50% MVC (D). The standard deviation of $\overline{N}$ across subjects is displayed with vertical bars. Two decomposition procedures were considered for the 256-electrode condition; the grid of 256 black electrodes indicates that the 256 signals were simultaneously decomposed and systematically returned lower $\overline{N}$ results than when the grid was decomposed as four subsets of 64 electrodes. To maintain consistency with the computational study, the trendlines were here fitted with the 4*64 condition that returned the higher number of identified motor units (see Extended Material A for the other fitting condition).

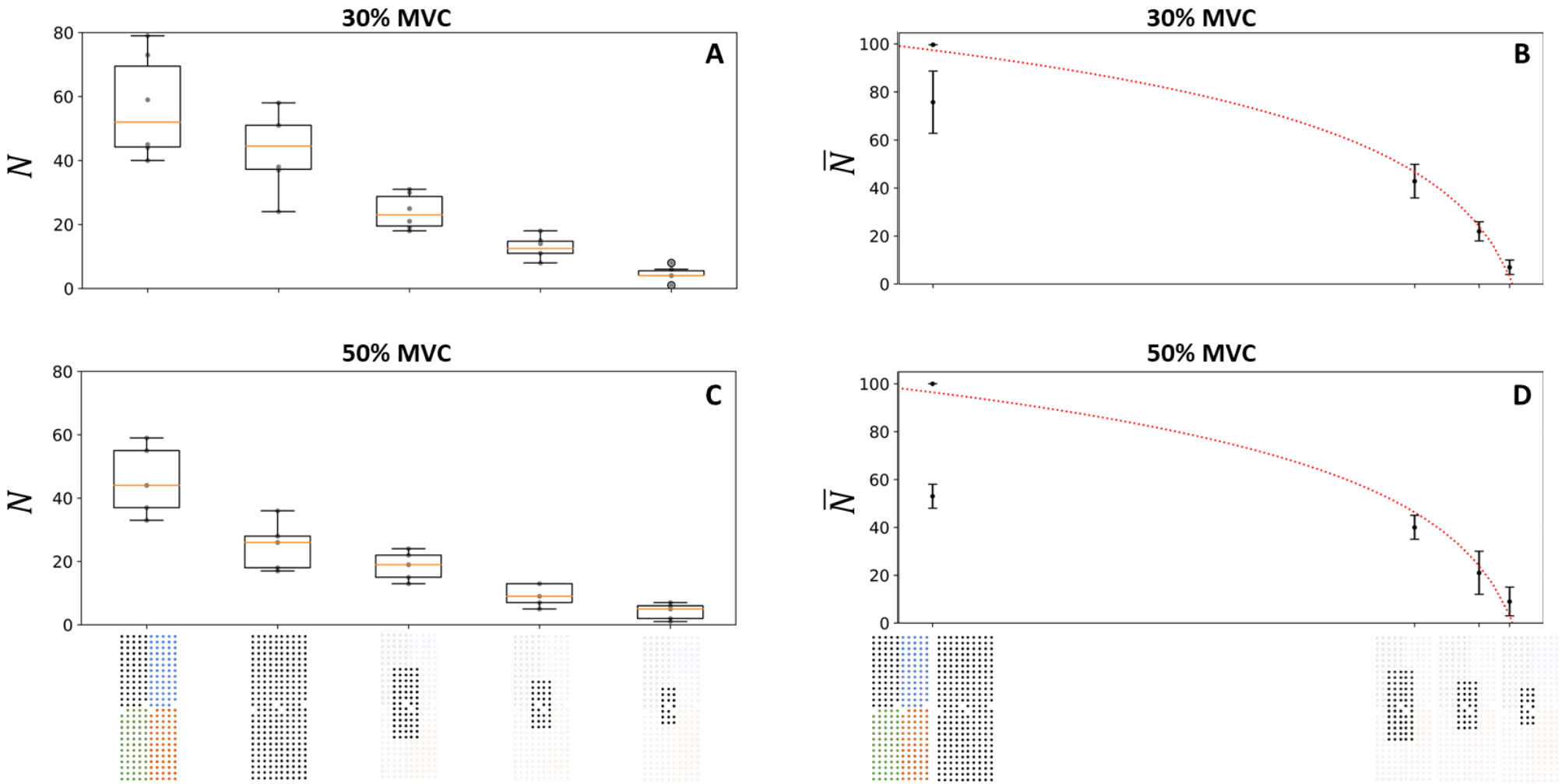

Figure 5: Effect of the size of the grid on the number of identified motor units N at 30% (A, B) and 50% MVC (C, D). The boxplots in the left column report the absolute number N of identified motor units per participant (grey dots) and the median (orange line), quartiles, and 95%-range across participants. In the right column, the normalized number of motor units $\bar{N}$ logarithmically decreases with the size of the grid s (2, 3.8, 7.7, and 36 cm^2 in abscissa) as $\bar{N} = -20 + 33\,log(s)$ $(r^2 = 0.99, p = 3.0 \cdot 10^{-4})$ at 30% MVC (B), and $\bar{N} = -19 + 32\,log(s)$ $(r^2 = 0.98, p = 0.001)$ at 50% MVC (D). The standard deviation of $\bar{N}$ across subjects is displayed with vertical bars. Two decomposition procedures were considered for the 256-electrode condition; the grid of 256 black electrodes indicates that the 256 signals were simultaneously decomposed and systematically returned lower $\bar{N}$ results than when the grid was decomposed as four subsets of 64 electrodes. To maintain consistency with the computational study, the trendlines were here fitted with the 4*64 condition that returned the higher number of identified motor units (see Extended Material A for the other fitting condition).

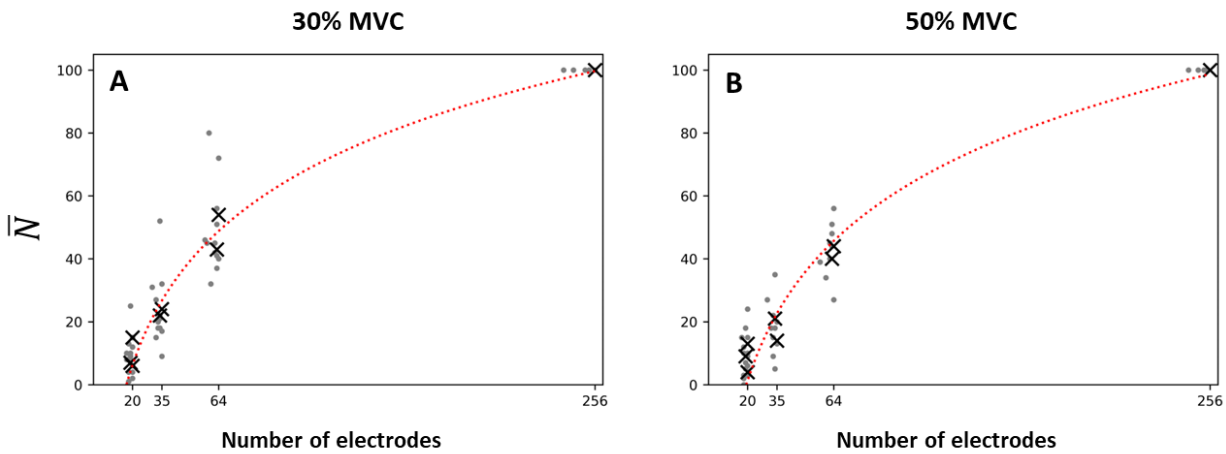

Figure 6: Effect of the number n of electrodes on the normalized number $\overline{N}$ of identified motor units at 30% (A) and 50% MVC (B). The discrete results per participant are displayed with grey data points. The average $\overline{N}$ values across participants per condition are displayed with black crosses. Weighted logarithmic trendlines were fitted to the data and returned (A) $\overline{N} = -104 + 37\,log(n)$ ($r^2 = 0.98, p = 0.018$), and (B) $\overline{N} = -113 + 38\,log(n)$ ($r^2 = 0.95,\ p = 0.016$). Two decomposition procedures were considered for the 256-electrode condition; the grid of 256 black electrodes indicates that the 256 signals were simultaneously decomposed and systematically returned lower $\overline{N}$ results than when the grid was decomposed as four subsets of 64 electrodes. To maintain consistency with the computational study, the trendlines were here fitted with the 4*64 condition that returned the higher number of identified motor units (see Extended Material A for the other fitting condition).

<u>Characteristics of identified motor units</u>

We found an increasing logarithmic relationship between the percentage of early recruited motor units for each participant and the density of the grid, with $r^2 = 0.91$ ($p = 2.8 \cdot 10^{-3}$) at 30% MVC (Figure 7F). Contrary to the density, the size of the grid did not impact the percentage of early recruited motor units, with the percentage ranging from 20 to 29% across all grid sizes and the logarithmic trendline fitting returning negligible slope and low $r^2 = 0.28$ (Figure 7C, G). Such differences were also not observed at 50% MVC, where the percentage of early recruited motor units remained below 10% for all conditions.

To support the above observations made at 30% MVC, grids involving the same number of electrodes but of different grid density and size were directly compared. 62% of the motor units identified with the 64-electrode (32 cm^2, IED 8 mm) and 63-electrode (7.7 cm^2, IED 4 mm) conditions were identified by both grids at 30%. 28 ± 9% of the remaining motor units specific to the 8-mm IED grid were early recruited, while 44 ± 11% of the motor units specific to the 4-mm IED condition were early recruited. Similar results were obtained with the 35- (36 cm^2, 12-mm IED) and 34-electrode conditions (3.6 cm^2, 4-mm IED), where a larger number of early recruited motor units were specifically identified with denser rather than larger grids.

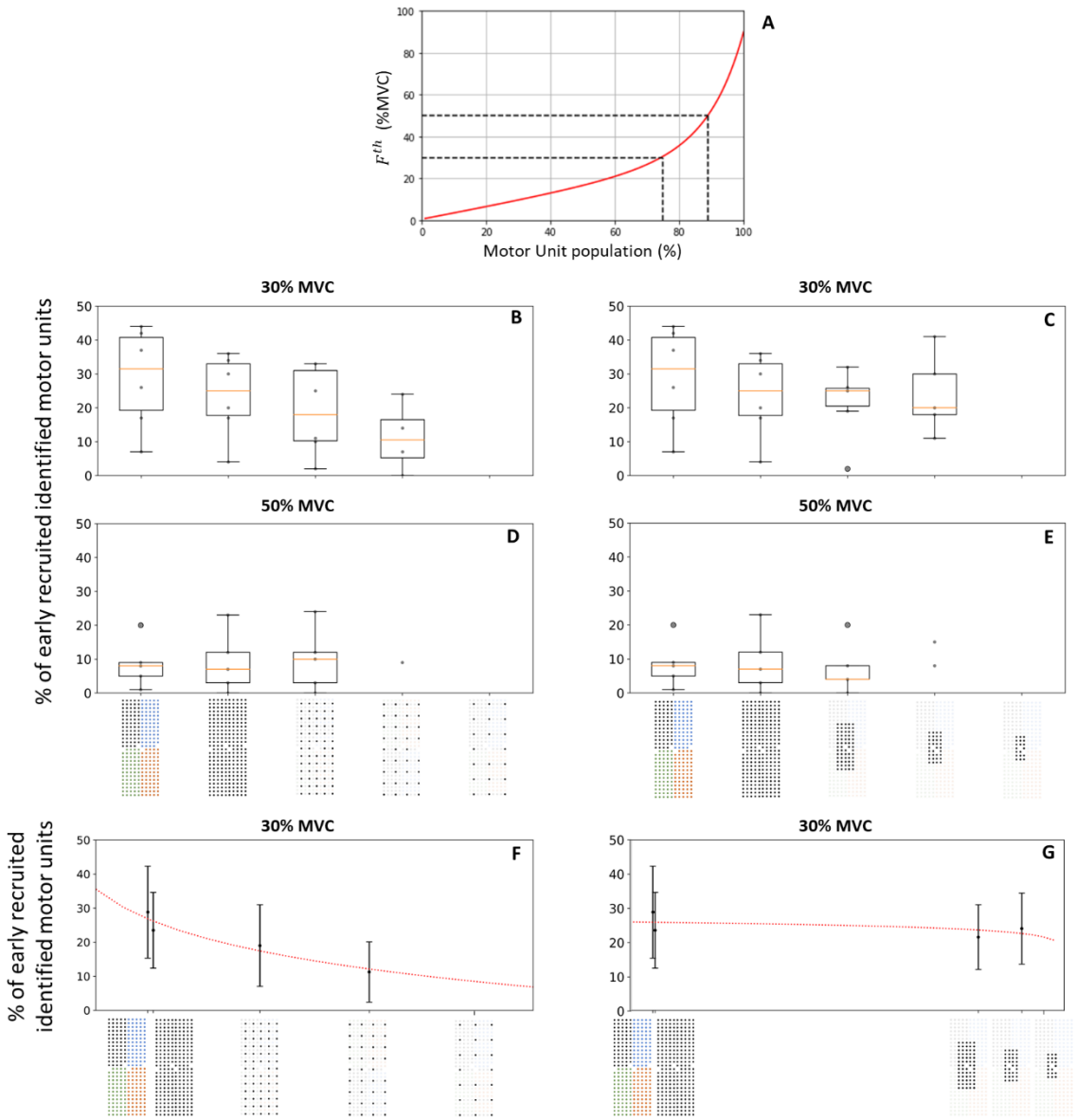

Figure 7: (A) Typical frequency distribution of motor unit force recruitment thresholds in a human TA motor unit pool ranked in ascending order of force recruitment thresholds according to the Methods. The black dashed lines identify the theoretical portions of the population recruited at 30% and 50% MVC. Effect of the grid density (B, D, F) and grid size (C, E, G) on the percentage of early recruited motor units identified at 30% (B, C, F, G) and 50% MVC (D, E). The boxplots report the results per participant (grey dots) and the median (orange line), quartiles, and 95%-range across participants. (F) At 30% MVC, the percentage of early recruited identified motor units logarithmically decreases with interelectrode distance d (4, 8, 12, and 16mm in abscissa) as $44.6 - 13.1\,log(d)$ $(r^2 = 0.91, p = 2.8 \cdot 10^{-3})$. (G) At 30% MVC, the percentage of early recruited identified motor units does not vary with the size of the grid s (2, 3.8, 7.7, and 36 cm^2 in abscissa), the logarithmic trendline fitting $(20.5 + 1.2\,log(s))$ returning a negligible slope and low $r^2 = 0.28$ $(p = 8 \cdot 10^{-4})$. The standard deviation across subjects is displayed with vertical bars. Two decomposition procedures were considered for the 256-electrode condition; the grid of 256 black electrodes indicates that the 256 signals were simultaneously decomposed and systematically returned lower percentages of early recruited motor unit than when the grid was decomposed as four subsets of 64 electrodes. To maintain consistency with the computational study, the trendlines were here fitted with the 4*64 condition that returned the higher

number of identified motor units. We did not report the results when five or fewer motor units were identified in one condition for three or more participants.

Correlation between MUAPs from adjacent electrodes

Figure 8 reports the effect of electrode density on the level of correlation ρ between MUAP recorded over adjacent electrodes for the six participants. The lowest average correlation coefficient ρ was observed with an IED of 16 mm (ρ = 0.87 ± 0.03 and ρ = 0.88 ± 0.04 at 30% and 50% MVC, respectively). The level of correlation increased with reduced IED (Figure 8B, C), with ρ = 0.96 ± 0.04 and ρ = 0.95 ± 0.05 between the MUAPs from adjacent electrodes with a 4-mm IED at 30% and 50% MVC, respectively.

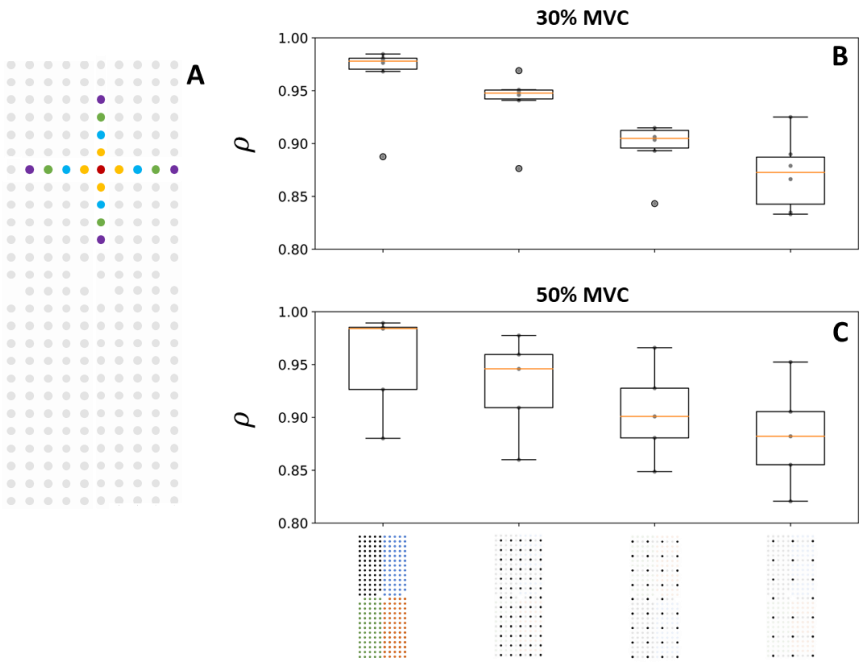

Figure 8: Effect of the electrode density on the correlation ρ between motor unit action potentials (MUAP) identified over adjacent electrodes (A) at 30% (B) and 50% MVC (C). The MUAP shape identified over the red electrode was compared to those identified over the four adjacent electrodes located at 4 (orange), 8 (blue), 12 (green) and 16 (purple) mm IED (A). The boxplots report the correlation coefficient ρ per participant (grey dots) and the median (orange line), quartiles, and 95%-range across participants.

Laboratory study with an ultra-dense prototyped grid of 256 electrodes with 2-mm IED

Maximal N of 31 and 26 motor units (PNR > 28 dB) were identified for one participant with the ultra-dense grid of 256 electrodes (2-mm IED, 9 cm^2, Figure 1H) at 30% and 50% MVC, respectively (Figure 9B). Note that the signals from four independent subsets of 64 electrodes were decomposed separately. For that participant, more motor units were identified with the ultra-dense grid of 256 electrodes than with the grid of 64 electrodes covering the same surface (Figure 5A, C). Indeed, 31 and 26 motor units

were respectively identified at 30% and 50% MVC with the grid of 256 electrodes (Figure 9C), while 25 (24 ± 5 for the group) and 19 (18 ± 4 for the group) motor units were identified (Figure 5A, C) with the grid of 64 electrodes (Figure 1E). Moreover, fewer motor units were identified when the electrode density of the ultra-dense grid was decreased (Figure 9C), with 22 and 13 motor units identified with a 4- and 8-mm IED at 30% MVC, respectively, and 21 and 9 motor units identified with a 4- and 8-mm IED at 50% MVC, respectively. At 30% MVC, the rate of increase of N between 4- and 2-mm IED followed the prediction computed in Figure 4B and illustrated by the dash line in Figure 9C. At 50% MVC, the rate of increase of N (dotted line in Figure 9C) was lower than the prediction. As previously observed, the correlation between adjacent MUAPs increased from $\rho = 0.92$ with an 8-mm IED to $\rho = 0.98$ with a 2-mm IED at 30% MVC, and from $\rho = 0.85$ with an 8-mm IED to $\rho = 0.93$ with a 2-mm IED at 50% MVC (Figure 9A). All the motor units identified with the 8-mm and 4-mm IED were also identified with the 4 mm and 2-mm IED grids, respectively. Finally, more motor units with an early recruitment were identified when increasing the density from a 8- to 4-mm IED (blue vs black trains in Figure 9B), and from 4- to 2-mm IED (red trains in Figure 9B).

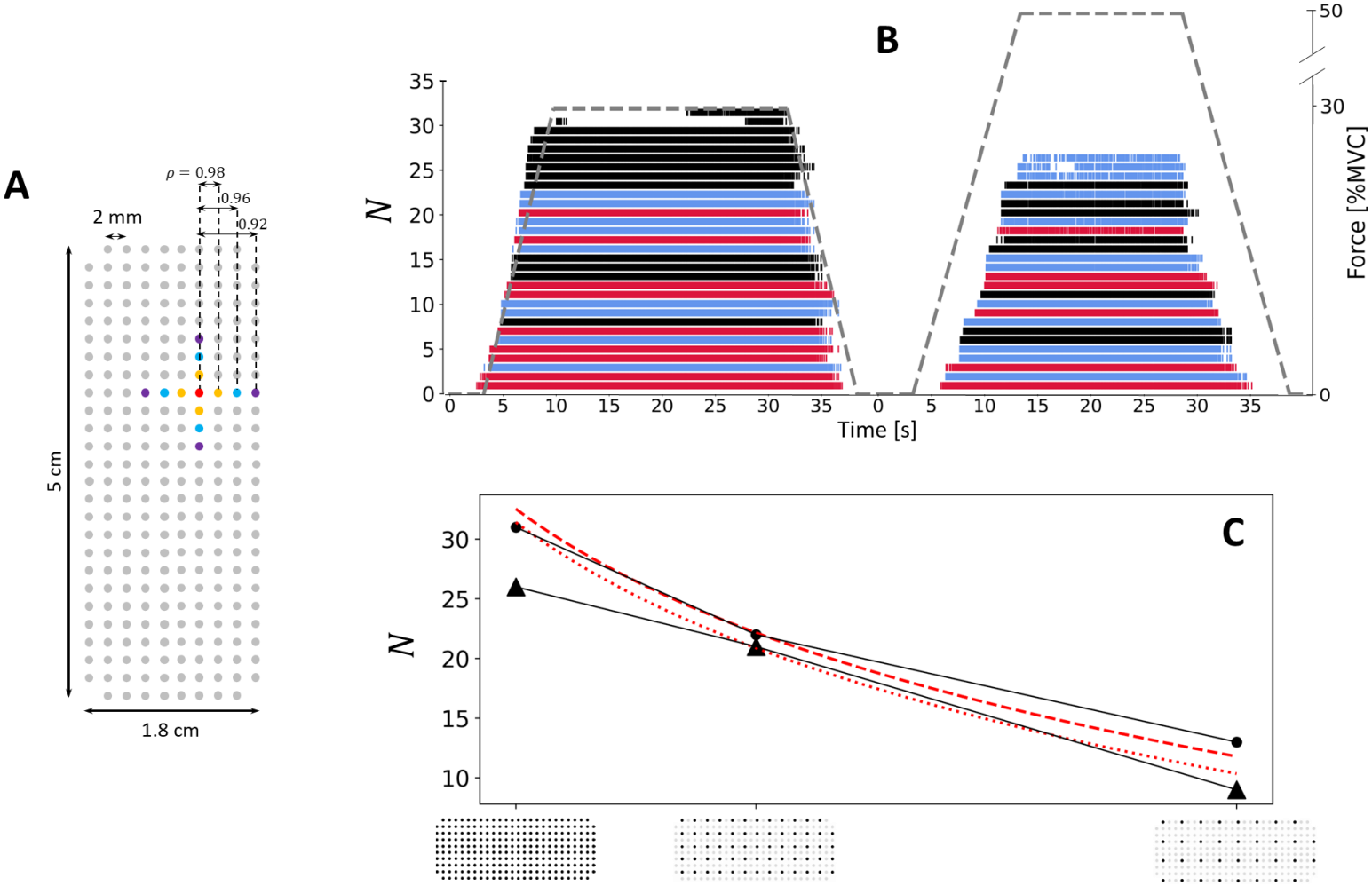

Figure 9: Results for the ultra-dense prototyped grid (2 mm IED, 5 x 1.8 cm, 256 electrodes). (A) Description of the ultra-dense grid (grey circles represent electrodes). On average, the correlation between MUAPs separated by an IED of 2 mm (orange), 4 mm (blue), and 8 mm (purple) from the MUAP with the highest peak-to-peak amplitude (red) reached ρ = 0.98, 0.96, and 0.92 at 30% MVC, respectively, and 0.93, 0.88, and 0.85 at 50% MVC, respectively. (B) Identified spike trains at 30% (left) and 50% MVC (right). The dark spike trains were identified with a 8 mm IED, the blue trains were additionally identified with a 4 mm IED, and the red trains were additionally identified with a 2 mm IED. All the spike trains identified with one grid were also identified with the denser grids. (C) Effect of electrode density on the number of identified motor units at 30% (scatters) and 50% MVC (triangles). The trendlines from the density analysis in Figure 4B, D are also reported (red dotted lines). To maintain consistency with the previous computational and laboratory results, the grid was decomposed as four independent subsets of 64 electrodes, as explained in the Methods, to identify the number of motor units.

Discussion

This study systematically investigated how the design of surface grids of EMG electrodes (grid size and electrode density) impacts the number and the characteristics of the motor units identified with EMG decomposition. Using a combination of computational and experimental approaches, we found that larger and denser grids of electrodes than conventionally used reveal a larger sample of motor units. As the motor units not identifiable with less dense and smaller grids mostly have an early recruitment threshold, we conclude that denser grids allow the identification of smaller motor units. This is possible because of a better spatial sampling of the MUAP distribution over the skin surface that resulted in a better discrimination among action potentials of different motor units. These results clarify the directions for designing new surface grids of electrodes that could span across the entire surface of the muscle of interest while keeping a high density of electrodes, with IED as low as 2 mm. Identifying large sets of small and large motor units is relevant in many research areas related to motor control, such as the investigation of neural synergies (Hug et al., 2022), neuromuscular modelling (Caillet et al., 2022c), or human-machine interfacing (Farina et al., 2021).

The number N of identified motor units increased across participants with the density of electrodes (Figure 4; Figure 8C), the size of the grid (Figure 5), and the number of electrodes (Figure 6). On average, 30 and 19 motor units were identified with the 'conventional' 64-electrode grid (8-mm IED, 32 cm^2 surface area) at 30% and 50% MVC, respectively, which is consistent with several previous studies using similar grid designs (Del Vecchio et al., 2020). By increasing the density of electrodes and size of the grid to reach a total of 256 electrodes separated by a 4-mm IED, we identified on average 56 and 45 motor units at 30% and 50% MVC, respectively. We even reached 79 and 59 motor units for one subject (Figure 3), which is substantially more than the numbers of motor units usually reported in the HD-EMG literature, and twice those obtained with grids of 64 electrodes in this study. Our computational and experimental results showed that the size of the grid is a key factor contributing to the higher number of identified motor units (Figure 2B; Figure 5). According to our simulations, increasing the size of the grid increases the number of identifiable motor units, i.e., the number of motor units with unique sets of MUAPs across electrodes (Figure 2B). We concluded from the simulation that the differences between MUAPs result from the anatomical and physiological differences between adjacent motor units, such as the length of their fibers, the spread of the end plates, or their conduction velocity, as well as from the differences in the tissues interposed between the fibers and each recording electrode (Farina et al., 2004). Larger grids better sample these differences across electrodes, revealing the unique shapes of each motor unit action potentials (Farina et al., 2008). The density of electrodes was also found to be a critical factor contributing to increasing the number of identified motor units (Figure 4; Figure 9C). Dense grids especially contribute to identifying the early recruited motor units.

Classically, the decomposition algorithms tend to converge towards the large and superficial motor units that contribute to most of the energy of the EMG signals (Farina and Holobar, 2016). Conversely, action potentials of the smallest motor units tend to have lower energy and are masked by the potentials of the larger units. These factors explain the lowest representation of low-threshold motor units in available HD-EMG datasets (Caillet et al., 2022a). Increasing the density of electrodes would therefore enable to better sample the action potentials of these early recruited motor units across multiple electrodes, enabling their identification. We however observed that increasing the electrode density did not reveal early recruited motor units during high-force muscle contractions (Figure 7D), potentially because of the large energy of the recorded MUAPs from the large motor units recruited between 30% and 50% MVC. We also showed in one subject that computationally increasing the density of electrodes by spatially resampling the experimental EMG signals did not reveal any previously hidden motor units (Extended Material B).

The number of identified motor units N monotonically increased with the density of electrodes (Figure 4BD), the size of the grid (Figure 5BD) and the number of electrodes (Figure 6), following significant logarithmic trendlines. Remarkably, very similar logarithmic tendencies were obtained at both 30% and 50% MVC in all the analyses. Altogether, these trendlines suggested that the normalized number of identified motor units $\overline{N}$ would grow with an electrode density beyond a 4-mm IED. We experimentally tested this hypothesis by designing a new prototyped grid of 256 electrodes separated by an IED of 2 mm. As predicted, more motor units were identified with a 2 mm than a 4 mm IED, following at 30% MVC the same rate of increase as the logarithmic trendlines (Figure 9C) between 4-mm and 2-mm IED. This increase may plateau with higher electrode densities, as the level of correlation between MUAPs identified over adjacent electrodes tended to 1 (Figure 9A). Therefore, the high level of information shared between adjacent electrodes in ultra-dense grids (IED < 2 mm) may limit the percentage of identifiable motor units (Farina and Holobar, 2016). According to these results, we consider that optimal designs of surface grids of electrodes for identifying individual motor units would involve a surface that cover the muscle of interest with an IED as low as 2 mm.

Another important factor for the identification of individual motor units is the quality of the identified pulse trains, estimated by the PNR (Holobar et al., 2014) or the silhouette value. In this study, we showed that the quality of the identified motor units (i.e., decomposition accuracy) increased when increasing the density of electrodes or the size of the grid, with PNR reaching on average 37-38 dB across participants with the grid of 256 electrodes (Extended Material C). A greater average PNR implies the need of less manual editing following the automatic decomposition (Hug et al., 2021b). The better spike train estimate depends on the better signal to noise ratio following the inversion of the mixing matrix

since the pulse train of each motor unit is computed by projecting the extended, whitened signals on the separation vector (Holobar and Farina, 2014; Farina and Holobar, 2016; Negro et al., 2016). Likewise, the PNR substantially increased after we computationally increased the number of electrodes by spatially resampling the EMG signals. This practical result is of interest for most of the physiological studies that require a lengthy processing time to visually check and manually correct the pulse trains of all the motor units (Hug et al., 2021b).

Finally, by independently decomposing subsets of 64 electrodes, we increased both the total number and the percentage of early recruited motor units identified from highly populated grids of 256 electrodes, compared to the simultaneous decomposition of all available observations (Figure 7B, C). This was likely due to the lower ratio of large motor units sampled by each subset of electrodes, allowing the algorithm to converge to smaller motor units that contributed to the signal (Figure 7B, C). According to Extended Material A, a plateauing behavior is expected to be observed when all the available signals are simultaneously decomposed. It should however be noted that the simulation results were obtained independently of a specific decomposition algorithm, as previously proposed by Farina et al (2008). On the other hand, the experimental results are based on a specific algorithm. Interestingly, however, the simulation and laboratory results were fully consistent and in agreement, indicating that the difference in shape of the spatially sampled MUAPs is the main factor influencing EMG decomposition.

Conclusion

By increasing the density and the number of electrodes, and the size of the grids, we increased the number of identifiable and experimentally identified motor units from the surface EMG. The identified motor units had pulse trains with high PNR, limiting the manual processing time. Moreover, we identified a higher percentage of early recruited motor units, which are classically filtered out with the current conventional grid designs. In this way, a maximum of 79 motor units (PNR > 28 dB; mean: 36 dB), including 40% of early recruited motor units, were identified, which is a substantially greater sample than previously shown with smaller and less dense grids. From these results, we encourage researchers to develop and apply larger and denser EMG grids to cover the full muscle of interest with IEDs as small as 2 mm. This approach increases the sample of motor units that can be experimentally investigated with non-invasive techniques.

References:

Afsharipour B, Ullah K, Merletti R (2015) Amplitude indicators and spatial aliasing in high density surface electromyography recordings. Biomedical Signal Processing and Control 22:170-179.

Caillet AH, Phillips ATM, Farina D, Modenese L (2022a) Estimation of the firing behaviour of a complete motoneuron pool by combining electromyography signal decomposition and realistic motoneuron modelling. PLoS Comput Biol 18:e1010556.

Caillet AH, Phillips ATM, Farina D, Modenese L (2022b) Mathematical relationships between spinal motoneuron properties. Elife 11.

Caillet AH, Phillips ATM, Carty CP, Farina D, Modenese L (2022c) Hill-type computational models of muscle-tendon actuators: a systematic review. bioRxiv:2022.2010.2014.512218.

Churchland MM, Shenoy KV (2007) Temporal complexity and heterogeneity of single-neuron activity in premotor and motor cortex. J Neurophysiol 97:4235-4257.

Del Vecchio A, Negro F, Felici F, Farina D (2017) Associations between motor unit action potential parameters and surface EMG features. J Appl Physiol (1985) 123:835-843.

Del Vecchio A, Holobar A, Falla D, Felici F, Enoka RM, Farina D (2020) Tutorial: Analysis of motor unit discharge characteristics from high-density surface EMG signals. J Electromyogr Kinesiol 53:102426.

Enoka RM (2019) Physiological validation of the decomposition of surface EMG signals. J Electromyogr Kinesiol 46:70-83.

Farina D, Holobar A (2016) Characterization of Human Motor Units From Surface EMG Decomposition. Proceedings of the Ieee 104:353-373.

Farina D, Merletti R, Enoka RM (2004) The extraction of neural strategies from the surface EMG. J Appl Physiol (1985) 96:1486-1495.

Farina D, Negro F, Gazzoni M, Enoka RM (2008) Detecting the unique representation of motor-unit action potentials in the surface electromyogram. J Neurophysiol 100:1223-1233.

Farina D, Negro F, Muceli S, Enoka RM (2016) Principles of Motor Unit Physiology Evolve With Advances in Technology. Physiology (Bethesda) 31:83-94.

Farina D, Vujaklija I, Brånemark R, Bull AMJ, Dietl H, Graimann B, Hargrove LJ, Hoffmann KP, Huang HH, Ingvarsson T, Janusson HB, Kristjánsson K, Kuiken T, Micera S, Stieglitz T, Sturma A, Tyler D, Weir RFF, Aszmann OC (2021) Toward higher-performance bionic limbs for wider clinical use. Nat Biomed Eng.

Gallego JA, Perich MG, Chowdhury RH, Solla SA, Miller LE (2020) Long-term stability of cortical population dynamics underlying consistent behavior. Nat Neurosci 23:260-270.

Heckman CJ, Enoka RM (2012) Motor unit. Compr Physiol 2:2629-2682.

Henneman E, Mendell LM (1981) Functional Organization of Motoneuron Pool and its Inputs. In: Comprehensive Physiology, pp 423-507.

Holobar A, Farina D (2014) Blind source identification from the multichannel surface electromyogram. Physiol Meas 35:R143-165.

Holobar A, Minetto MA, Farina D (2014) Accurate identification of motor unit discharge patterns from high-density surface EMG and validation with a novel signal-based performance metric. J Neural Eng 11:016008.

Hug F, Del Vecchio A, Avrillon S, Farina D, Tucker K (2021a) Muscles from the same muscle group do not necessarily share common drive: evidence from the human triceps surae. J Appl Physiol (1985) 130:342-354.

Hug F, Avrillon S, Sarcher A, Del Vecchio A, Farina D (2022) Correlation networks of spinal motor neurons that innervate lower limb muscles during a multi-joint isometric task. J Physiol.

Hug F, Avrillon S, Del Vecchio A, Casolo A, Ibanez J, Nuccio S, Rossato J, Holobar A, Farina D (2021b) Analysis of motor unit spike trains estimated from high-density surface electromyography is highly reliable across operators. J Electromyogr Kinesiol 58:102548.

Jun JJ et al. (2017) Fully integrated silicon probes for high-density recording of neural activity. Nature 551:232-236.

Konstantin A, Yu T, Le Carpentier E, Aoustin Y, Farina D (2020) Simulation of Motor Unit Action Potential Recordings From Intramuscular Multichannel Scanning Electrodes. IEEE Transactions on Biomedical Engineering 67:2005-2014.

Muceli S, Poppendieck W, Holobar A, Gandevia S, Liebetanz D, Farina D (2022) Blind identification of the spinal cord output in humans with high-density electrode arrays implanted in muscles. Science advances 8:eabo5040.

Muceli S, Poppendieck W, Negro F, Yoshida K, Hoffmann KP, Butler JE, Gandevia SC, Farina D (2015) Accurate and representative decoding of the neural drive to muscles in humans with multi-channel intramuscular thin-film electrodes. J Physiol 593:3789-3804.

Negro F, Muceli S, Castronovo AM, Holobar A, Farina D (2016) Multi-channel intramuscular and surface EMG decomposition by convolutive blind source separation. J Neural Eng 13:026027.

Steinmetz NA, Koch C, Harris KD, Carandini M (2018) Challenges and opportunities for large-scale electrophysiology with Neuropixels probes. Curr Opin Neurobiol 50:92-100.

Stringer C, Pachitariu M, Steinmetz N, Reddy CB, Carandini M, Harris KD (2019) Spontaneous behaviors drive multidimensional, brainwide activity. Science 364:255.

EXTENDED MATERIAL

A. Laboratory study – number of identified motor units when all signals are simultaneously decomposed

Methods

As described in the Methods of the main manuscript, we decomposed separate subsets of 64 electrodes in addition to the decomposition of the full grid of 256 electrodes. We systematically found that the decomposition of subsets returned a higher number of identified motor units. These results were provided in the main document to maintain consistency with the computational study that aimed to investigate the highest number of identifiable motor units depending on the design of the grid. Here, we fitted logarithmic trendlines between the averaged $\bar{N}$ values and IED, grid size, and number of channels, as in Figures 4, 5, and 6 of the main document. The trendlines were however fitted with the values obtained from the decomposition of the full grid of 256 electrodes.

Results

We found the highest number of motor units with the highest density (4-mm IED) and the largest surface (36 cm^2). Every time, the decomposition with separate subsets of 64 electrodes identified more motor units than the decomposition of the full set of 256 electrodes. Specifically, 56 ± 14 vs. 43 ± 11 motor units and 45 ± 10 vs. 25 ± 6 motor units were identified with an IED of 4mm at 30% and 50% MVC with the 4×64 vs. the 256-electrode decomposition, respectively. 56 ± 14 vs. 43 ± 11 motor units and 45 ± 10 vs. 25 ± 6 motor units were identified with a surface of 36 cm^2 at 30% and 50% MVC, with the 4×64 vs. the 256-electrode decomposition, respectively.

Consistent with the results provided in the main document, $\bar{N}$ increased with electrode density (d), grid size (s), and with the number of electrodes (n) (Figure A.1.) following statistically significant logarithmic trendlines ($p < 0.05$). At 30% MVC, $\bar{N} = 198 - 67\,log(d)$ ($r^2 = 0.92$), $\bar{N} = -10 + 31\,log(s)$ ($r^2 = 0.98$), and $\bar{N} = -78 + 32\,log(n)$ ($r^2 = 0.90$). At 50% MVC, $\bar{N} = 204 - 69\,log(d)$ ($r^2 = 0.92$), $\bar{N} = 5 + 28\,log(s)$ ($r^2 = 0.98$), and $\bar{N} = -57 + 29\,log(n)$ ($r^2 = 0.90$).

Although the logarithmic function provided the best fits for the results reported in the main manuscript, with $r^2 > 0.95$, and was maintained here for consistency, other more suitable functions, such as sigmoid or $y = a + b \cdot \log(x^c)$ functions, could have been proposed in Figure A.1. to better predict the plateau reached with high d, s, and n values. It is noteworthy that the trendlines exhibited more pronounced plateaus (lower b value in the $y = a + b \cdot \log(x)$ trendlines) with the decomposition of the full grid of 256 electrodes than with the decomposition of subsets of 64 electrodes.

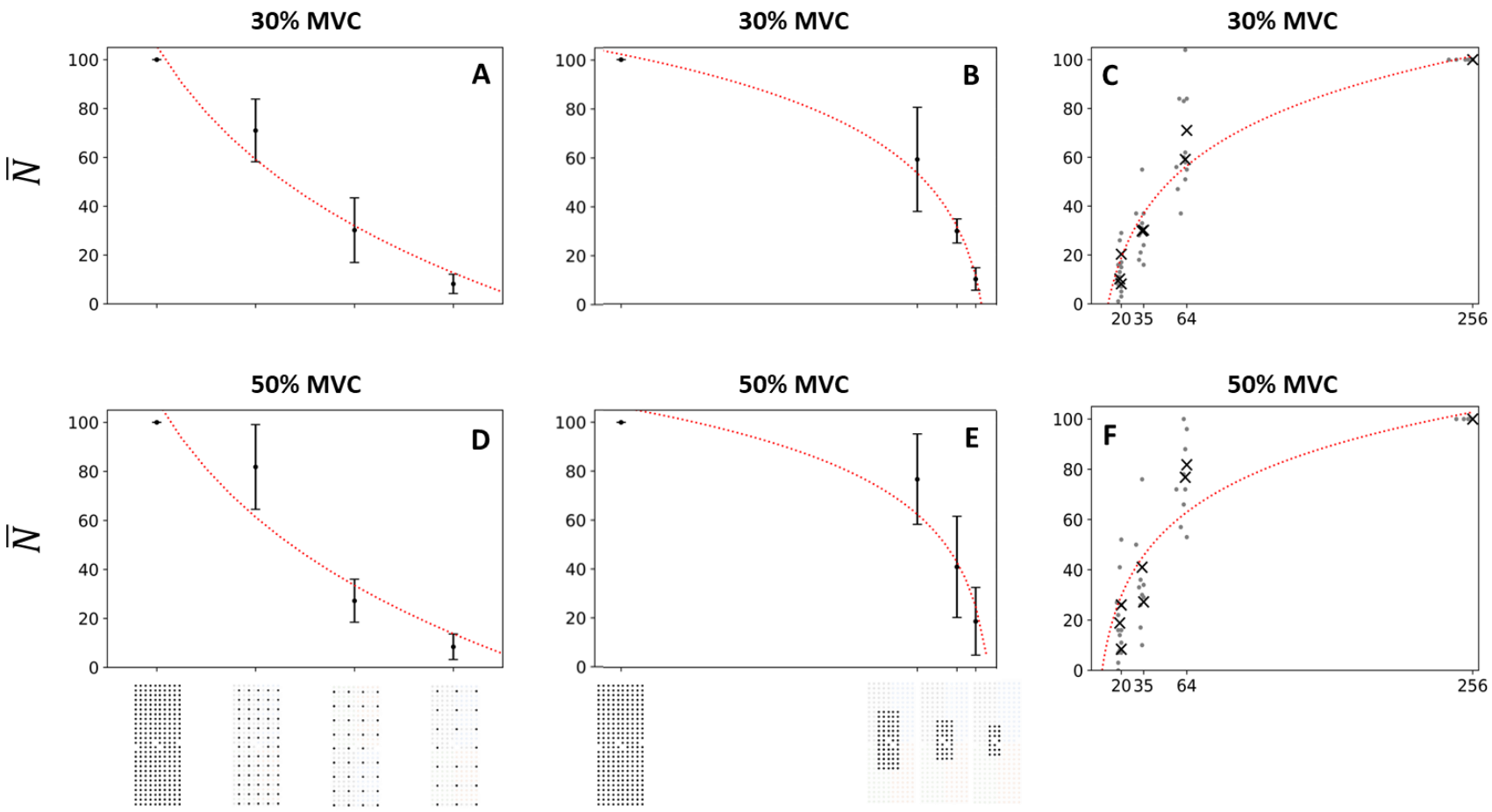

Figure A.1. Effect of the density of the grid (A, D), the size of the grid (B, D), and the number of electrodes (C, F) on the normalized number $\overline{N}$ of identified motor units at 30% (A, B, C) and 50% MVC (D, E, F). $\overline{N}$ was estimated after decomposing the full grid of 256 electrodes and manually editing the motor unit spike trains. Vertical bars (A, B, D, E) are the standard deviation of $\overline{N}$ across subjects, scatters are the individual data points, and crosses are their mean (C, F).

B. Laboratory study – spatial interpolation

Methods

We assessed whether generating denser grids of electrodes with a spatial mathematically interpolation of the EMG signals improved the identification of individual motor units. The signals recorded with the ultra-dense grid of 400 electrodes at 30% MVC were used for this analysis. Down-sampled montages of 5x5 electrodes with an IED of 8 mm and 10x10 electrodes with an IED of 4 mm were interpolated to generate 10x10 (4-mm IED) and 20x20 (2-mm IED) grids of electrodes, respectively. In these interpolated grids, 25% of the signals were therefore experimentally recorded and 75% interpolated. The spatial interpolation was performed at each time step with a two-dimensional *sinc* function (Afsharipour et al., 2015). We compared the pairs of 10x10 (4-mm IED) and 20x20 (2-mm IED) interpolated and experimentally recorded grids of electrodes by computing the correlation coefficient ρ between the signals for each electrode. Then, we compared the motor units identified with blind source separation between the interpolated and experimentally recorded grids of electrodes.

Results

The experimentally recorded and interpolated signals reached a correlation coefficient of $\rho = 0.90 \pm 0.08$ with an IED of 4mm. A better signal reconstruction was obtained with the 2 mm IED, with a correlation coefficient of $\rho = 0.93 \pm 0.09$ between recorded and interpolated signals. We identified 4 and 19 motor units from the interpolated grid with a 4-mm and 2-mm IED, respectively, vs. 19 and 24 motor units with the experimentally recorded signals. We only identified the same motor units as identified with the original less dense grids used to generate the interpolation. These results indicate that interpolation is not sufficient to reconstruct signals from a lower spatial sampling. This may be due to the spatial bandwidth which is greater than the inverse of the minimal interelectrode distance used or to the edge effects of the interpolation due to the relatively small size of the grid.

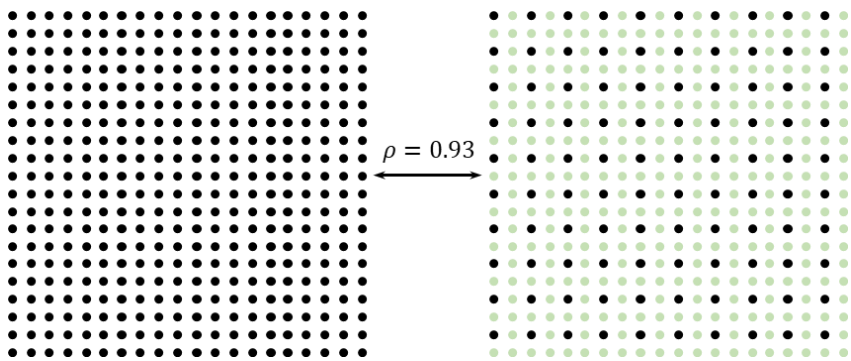

Figure B.1. Correlation ρ between experimentally recorded (Left, black) and interpolated (Right, green) EMG signals with a spatial resampling *sinc* function of the 100-channel 4-mm IED grid (Right, black).

683 C. Laboratory study – quality of the identified spike trains

684 Methods

685 An important factor for the identification of individual motor units is the quality of the identified pulse
686 trains, estimated by the PNR (Holobar et al., 2014) or the silhouette value (Negro et al., 2016) (Holobar
687 et al., 2014; Hug et al., 2021b). We calculated the average PNR value for the motor unit spike trains
688 (PNR > 28 dB) identified in each subject and condition.

689 Results

690 The average PNR across identified motor units increased together with the density of the grid. The
691 lowest PNR values were observed with 16 mm-IED, i.e., 30 ± 1.8 dB at 30% MVC and 29 ± 1.2 dB at
692 50% MVC. The highest PNR was observed with 4 mm-IED, i.e., 36 ± 0.8 dB at 30% MVC and 37 ±
693 0.7 dB at 50% MVC, enabling the operators to quickly edit the identified motor units.

694 Similarly, the PNR increased together with the size of the grid. The lowest PNR were observed with a
695 grid of 2 cm^2 (31 ± 0.9 dB at 30% MVC and 30 ± 0.9 dB at 50% MVC). The highest PNRs were observed
696 with a grid of 36 cm^2 (36 ± 0.7 dB at 30% MVC and 37 ± 0.7 dB at 50% MVC).

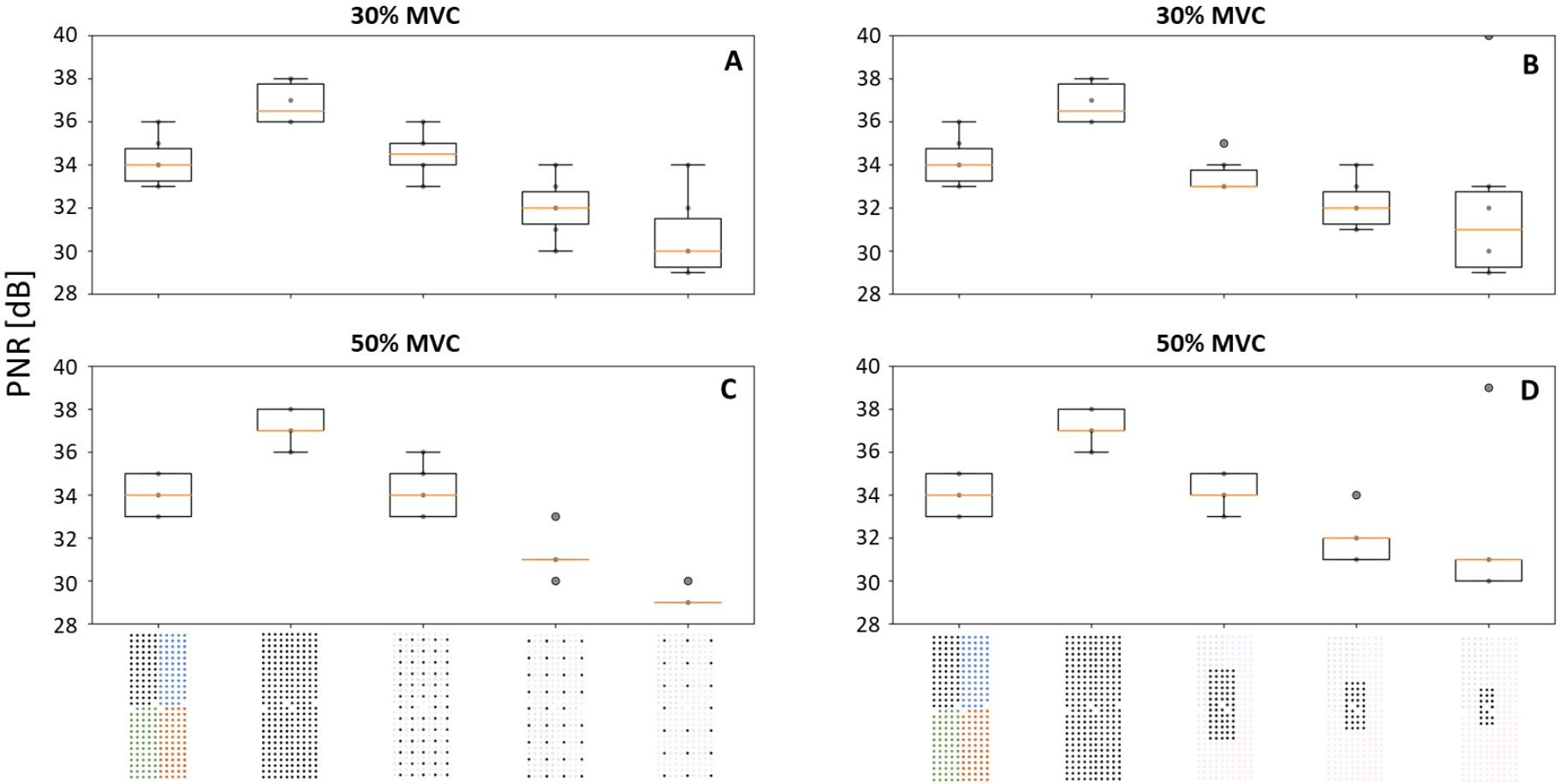

Figure C.1. Effect of the electrode density (A, C) and grid size (B, D) on the average PNR across the identified spike trains at 30% MVC (A, B) and 50% MVC (C, D). The boxplots report the average PNRs per participant (grey dots) and the median (orange line), quartiles, and 95%-range across participants.